Systems/Circuits

Phase Locking of Multiple Single Neurons to the Local Field Potential in Cat V1

Kevan A. C. Martin and Sylvia Schröder
Institute of Neuroinformatics, University of Zürich, and ETH Zürich, 8057 Zürich, Switzerland

The local field potential (LFP) is thought to reflect a temporal reference for neuronal spiking, which may facilitate information coding and orchestrate the communication between neural populations. To explore this proposed role, we recorded the LFP and simultaneously the spike activity of one to three nearby neurons in V1 of anesthetized cats during the presentation of drifting sinusoidal gratings, binary dense noise stimuli, and natural movies. In all stimulus conditions and during spontaneous activity, the average LFP power at frequencies >20 Hz was higher when neurons were spiking versus not spiking. The spikes were weakly but significantly phase locked to all frequencies of the LFP. The average spike phase of the LFP was stable across high and low levels of LFP power, but the strength of phase locking at low frequencies (≤10 Hz) increased with increasing LFP power. In a next step, we studied how strong stimulus responses of single neurons are reflected in the LFP and the LFP–spike relationship. We found that LFP power was slightly increased and phase locking was slightly stronger during strong compared with weak stimulus-locked responses. In summary, the coupling strength between high frequencies of the LFP and spikes was not strongly modulated by LFP power, which is thought to reflect spiking synchrony, nor was it strongly influenced by how strongly the neuron was driven by the stimulus. Furthermore, a comparison between neighboring neurons showed no clustering of preferred LFP phase. We argue that hypotheses on the relevance of phase locking in their current form are inconsistent with our findings.

Key words: **local field potential; natural stimuli; neighboring neurons; neural communication; phase locking; primary visual cortex**

Significance Statement

The local field potential (LFP) is hypothesized to play a vital role in the efficient communication between neuronal populations, as well as in the efficient coding of information. Underlying these roles is the assumption that spikes can be strongly and reliably locked to certain phases of oscillations in the LFP. Gamma oscillations are thought to be the best candidate mechanism exerting the hypothesized roles of the LFP. They occur most reliably in response to specific artificial stimuli, but are usually very weak in response to natural movies or images. The current study finds that spikes exhibited weak phase locking when the power of gamma oscillations is weak and thus casts doubt on a general relevance of phase locking for neural communication and coding.

Introduction

The local field potential (LFP) is the extracellular voltage measured in the frequency range below a few hundred Hertz. It is generated by electric currents contributed from all active cellular processes within a local volume of brain tissue (Buzsáki et al., 2012) and oscillations of the LFP are thought to reflect synchrony within neural populations (Buzsáki, 2006; Lindén et al., 2011). Although such oscillations may generate temporal "windows of opportunity" for neurons to spike (Buzsáki, 2006), their functional role is still debated.

One causal view, termed "communication through coherence" (Fries, 2005), is the hypothesis that oscillations are a means of enhancing communication between distant neuronal populations. If the LFPs and spikes of two populations oscillate coherently, then their communication can be maximized if spikes sent by one population arrive during the time window of maximal sensitivity in the other population (Fries, 2005; Womelsdorf et al., 2007). In a second hypothesis, termed "gamma-phase decoding" (Fries et al., 2007), oscillations in the gamma frequency (30–80 Hz) serve as a temporal reference frame where the phase at which a spike occurs encodes stimulus strength. These hypoth-

Received June 21, 2014; revised Jan. 15, 2016; accepted Jan. 19, 2016.

Author contributions: K.A.C.M. and S.S. designed research; K.A.C.M. and S.S. performed research; S.S. contributed unpublished reagents/analytic tools; S.S. analyzed data; K.A.C.M. and S.S. wrote the paper.

This work was supported by the European Union (Daisy Grant FP6 015803 and Grant EU SECO FP7 216593 to K.A.C.M.) and ETH Zürich (Grant 2-73246-08 to K.A.C.M.). We thank Nuno M. da Costa and Elisha Ruesch for help in performing the experiments; Sepp Kollmorgen for many discussions on data analysis; John Anderson, Andreas Keller, and Isabelle Spühler for support during the experiments; and Simone Rickauer for help with histological processing.

The authors declare no competing financial interests.

Correspondence should be addressed to Sylvia Schröder, UCL Institute of Ophthalmology, University College London, 11-43 Bath Street, London EC1V 9EL, UK. E-mail: sylvia.schroeder@ucl.ac.uk.

DOI:10.1523/JNEUROSCI.2547-14.2016

 0270-6474/16/362494-09$15.00/0

eses are not mutually exclusive and they offer general mechanisms for neuronal communication and coding.

An important condition underlying these two hypotheses is that spikes are tightly locked to a certain phase of the local LFP, at least when the local neural population is actively involved in representing or transmitting stimulus information. In response to different stimulus conditions, a neuron has to lock to a different phase of the LFP or exhibit weaker phase locking so that different stimuli can be distinguished and so that transmission of one stimulus does not interfere with that of another stimulus.

Oscillations at gamma frequencies are thought to be the best means of exerting phase locking because the mechanism that generates gamma frequencies could support a phase-of-firing code (Fries et al., 2007). Gamma oscillations are correlated with stimulus drive and with higher cognitive functions such as attention (Gray and Singer, 1989; Fries et al., 2001; Fries, 2009; Harris and Thiele, 2011; Jia and Kohn, 2011). Gamma oscillations are identified by a distinct peak in the power spectrum between 30 and 80 Hz, not simply a broadband elevation of power (Ray and Maunsell, 2011a; Buzsáki and Wang, 2012). They are commonly observed in response to specific visual stimuli, for example, large, high-contrast gratings (Gray et al., 1989; Frien et al., 2000; Henrie and Shapley, 2005; Gieselmann and Thiele, 2008; Jia et al., 2013b), but are not reliably evoked in response to other visual stimuli, including natural images and movies (Kayser et al., 2003; Siegel and König, 2003; supplemental Figure 8 in Haslinger et al., 2012; Hermes et al., 2015; but see Brunet et al., 2015). We therefore wanted to test the hypotheses of communication through coherence and gamma-phase decoding under conditions in which gamma oscillations are not especially prominent. By recording spikes from closely adjacent cells as well as the LFP, we identified conditions under which some key predictions of the hypotheses are not supported.

Materials and Methods

Animal preparation

All experiments, animal treatments, and surgical protocols were performed with authorization and under a license granted to K.A.C.M. by the Cantonal Veterinary Office of Zürich, Switzerland. The data presented here originate from 15 adult cats (2.2–4.3 kg) of either sex. The animals were initially anesthetized with a subcutaneous injection of xylazine (~0.5 mg/kg, Rompun 2%; Bayer) and ketamine (~15 mg/kg, Narketan 10, Vétoquinol). The femoral vein and artery and the trachea were cannulated while the cat was maintained under general anesthesia with ~2% halothane (Arovet) in oxygen/nitrous oxide (50%:50%) and with regular intravenous injections of alfaxalone/alfadolone (Saffan; Schering-Plough Animal Health). Throughout the experiment alfaxalone/alfadolone (~5–14 mg/kg/h and 2–5 mg/kg/h, respectively; Saffan; Schering-Plough Animal Health) was continuously delivered intravenously to maintain general anesthesia. The cat was artificially ventilated with oxygen/nitrous oxide (30%:70%) and the ventilation volume was adjusted so that end-tidal CO_2 remained at a level of ~4.5%. After opening the skull, the cat was given an intravenous injection of the muscle relaxant gallamine triethiodide (40 mg; Sigma-Aldrich) and thereafter gallamine triethiodide (~7.3 mg/kg/h; Sigma-Aldrich) mixed with (+)-tubocurarine chloride hydrate (~0.7 mg/kg/h; Sigma-Aldrich) was delivered intravenously to prevent eye movements. Lidocaine gel (4%; G. Streuli) was applied to all pressure points (ear bars and rectal thermometer). Topical antibiotics (Voltamicin; OmniVision) and atropine (1%; Ursapharm) to prevent accommodation was applied to the eyes before they were covered with gas-permeable, neutral power contact lenses. The nictitating membranes were retracted with phenylephrine (5%; Bausch & Lomb). During the course of the experiment, EEG (maintained in spindling state), ECG, and blood pressure (measured via cannula in femoral artery) were monitored continuously. If needed, additional intravenous Saffan injections or halothane (0–2%; Arovet) was given. A thermistor-controlled heating blanket, on which the cat was lying, kept the cat's rectal temperature at 37°C.

The location of the blind spot of each eye was marked on the screen used for mapping the receptive fields of the recorded neurons. This allowed the position of the area centralis to be estimated for each eye. Appropriate spectacle lenses were used to focus the eyes onto the screen positioned 114 cm in front of the eyes. A small craniotomy was performed over area 17 (Horsley–Clark coordinates anteroposterior −3 to −6 and mediolateral 0–3). A recording chamber was mounted over the craniotomy and a tiny durotomy was made at the recording site. After the recording electrode was lowered to the surface of the brain, the chamber was filled with agar (Sigma-Aldrich) for stabilization.

Electrophysiology

Spikes of single neurons were recorded using a glass micropipette with a tip diameter of 2–4 μm (for 4 recordings, the tip was beveled), filled with 1 mol/L potassium acetate (in a few cases with 0.05 mol/L Tris and 0.2 mol/L KCl with 2% of horseradish peroxidase), and signals were led to the preamplifier by means of a chlorided silver wire electrode. The pipettes had an average resistance of 25 MΩ (range of 6–90 MΩ). A second low-impedance glass pipette was used to record the local field potential. It was filled with a solution of 2% Pontamine Sky Blue (6B; Sigma-Aldrich) in 0.5 mol/L NaCl, 0.5 mol/L potassium acetate, and 0.01 mol/L phosphate buffer. The pipette had a mean tip diameter of 10 μm (range 3–14 μm) and a mean resistance of 4.4 MΩ (range 2–14 MΩ). The second pipette was glued to the high-impedance pipette at an average tip-to-tip distance of 34 μm (range 16–60 μm). Each electrode was optimized for its purpose: high impedance increased the signal-to-noise ratio when recording spikes and warranted that the recorded neurons were very close to the tip of the electrode; a low-impedance electrode is thought to be more suitable for picking up low-frequency signals, although the effects of electrode geometry on the recorded signal is still debated (Nelson and Pouget, 2010). In addition, using separate electrodes to record the LFP and spikes has the advantage that the LFP signal may be less contaminated by simultaneously recorded spikes.

The reference electrode (chlorided silver wire) for the recordings was attached to the scalp a few centimeters from the recording chamber. The signals of both recording electrodes were recorded with an Axoprobe-1A system (Molecular Devices), further amplified, and filtered, the spike signal on the high-impedance electrode in a band of 100–8000 Hz (filter by NeuroLog Systems) and the LFP signal on the low-impedance electrode in a band of 1–400 Hz (filter by Kemo). Both signals were then digitized with a 12-bit resolution, the spike signal at 20 kHz and the LFP signal at 1 kHz (CED 1401 and Spike2 software; CED).

Visual stimuli

The receptive field of one or more cells were plotted by hand and location, size, ocular dominance, orientation, and direction preference and the receptive field types (simple or complex) were determined. The centers of the receptive fields had an average distance of ~4° (always <10°) from the area centralis positions (estimated from the blind spots) and an average size of 1.25° (along preferred orientation) × 1.2° (orthogonal to preferred orientation). Computer-generated stimuli were then presented on a Sony CPD-G500 monitor under control of a ViSaGe graphics card (Cambridge Research Systems). The monitor placed at 114 cm in front of the cat's eyes had an image area of 19.1° × 14.4° at a resolution of 800 × 600 pixels. Minimum and maximum luminance values were 0.39 cd/m^2 and 101.31 cd/m^2, respectively. The frame rate was 100 Hz. All stimuli were centered approximately on the center of the hand-plotted receptive field and extended well beyond the classical receptive fields of the recorded neurons and were presented monocularly to the dominant eye (except in two cases in which only binocular stimulation was effective).

Sinusoidal drifting gratings were presented in a square aperture with edge lengths of 4°-6° on a mean gray background. Gratings were first varied in orientation and direction (in most cases), then in spatial frequency, and then in temporal frequency using appropriate step sizes and ranges depending on the selectivity of the neurons. Gratings were presented at low contrasts of 10–50% to prevent response saturation. They were shown for 5 s (in 3 recordings for 3 s) and were interleaved for 2 s (in

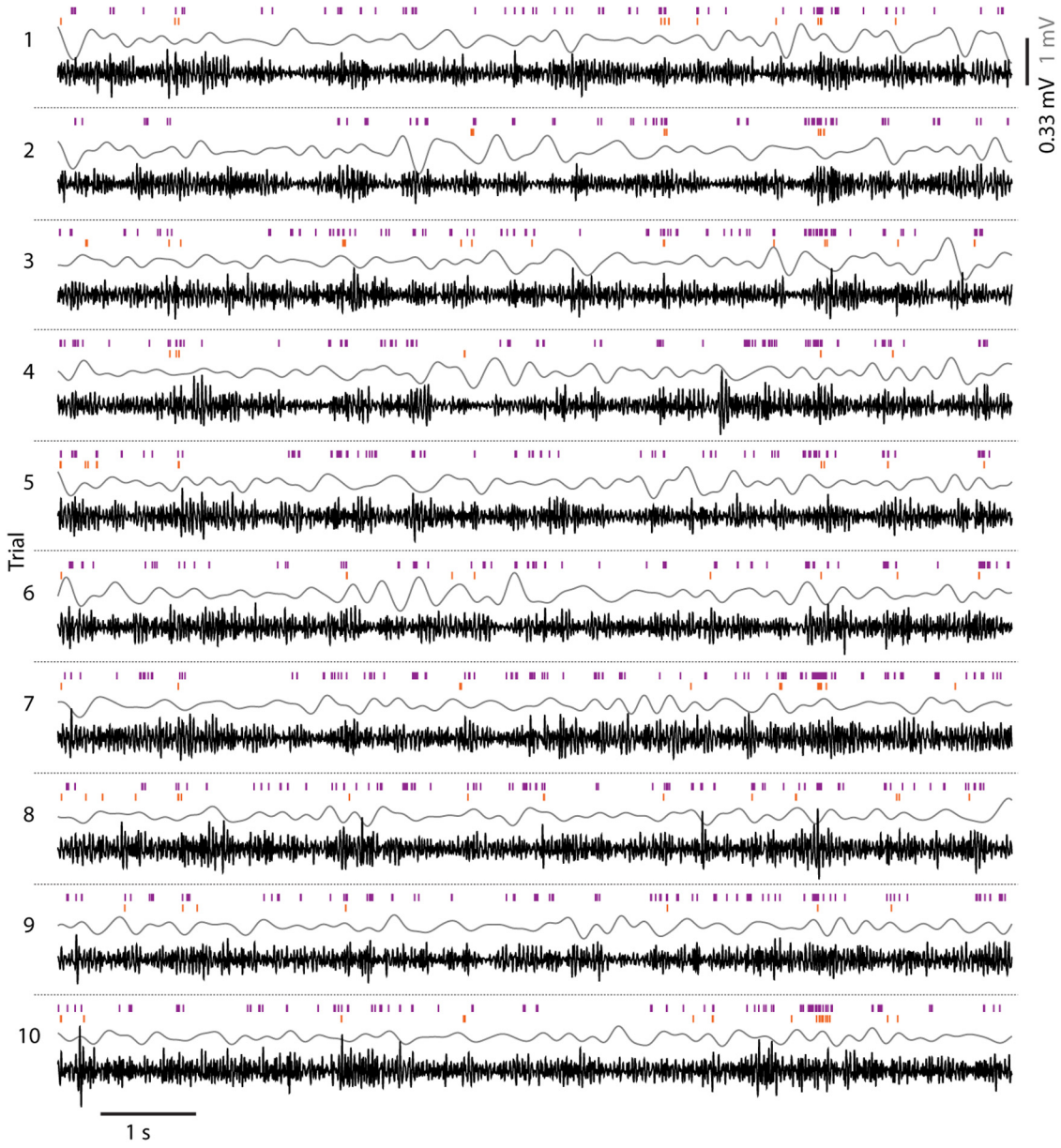

Figure 1. Example showing the relationship between LFP power and spikes in response to 10 repetitions of a natural movie (data from cat1310 P2C2). Spike times of two neurons (purple and orange tick marks, respectively) and the LFP filtered in two bands (gray: 1–4 Hz, black: 20–100 Hz) are depicted. Scale bar, 1.0 mV for the low-frequency LFP and 0.33 mV for the high-frequency LFP.

1 case for 10 s) with a blank mean gray screen. Gratings were presented in random order and each one was, in most cases, repeated 10 times (but at least 5 times) except when the recording had to be stopped prematurely due to loss of cells.

The natural movie scenes were digitized broadcasts from Dutch, British, and German television taken from Hans van Hateren's image and movie database (van Hateren and Ruderman, 1998). The movie images had a resolution of 128 × 128 pixels. To get an image size of 6.17° × 6.17°, each frame was magnified to 256 × 256 pixels by quadruplicating each pixel. Gray scale values of each movie were discretized to 255 values and scaled so that the brightest and darkest pixels reached maximal and minimal luminance, respectively. The movies were placed on a mean gray background and presented at 50 Hz (the original frame rate of the movies in the database) or at 25 Hz (after averaging pairs of consecutive frames). The power spectra elicited in response to movies of both frame rates were not significantly different from each other for any frequency band (*t* test, $n = 5$ for 25 Hz, $n = 23$ for 50 Hz). Each movie clip lasted for 10 s, contained no video cuts, and was repeated 30 times (in four pair recordings, movies were repeated only 10–20 times). The clips were interleaved by 3.7–4.5 s of a blank mean gray screen. For neurons that were lost before the presentation was completed, only data for movies (or parts thereof) that were presented for at least five trials were considered in further analyses.

The third stimulus type was binary dense noise consisting of elongated bars at an orientation intermediate between the preferred orientations of the neurons. The bars occurred in a grid with one to four rows and five to 15 columns. The grid had a width of 2.6–6° and a height of 2.4–5.3° and appeared on a mean gray background. Each image was presented for 20 ms; that is, for two video frames. The sequence of images was produced by changing the luminance value of each bar between white and black according to a pseudorandom binary m-sequence of order 12 (Victor, 1992). The same sequence was used for each bar, but was temporally shifted so that luminance values of all bars were uncorrelated to each other (shifts were determined as the ratio between the total length of the m-sequence in frames and the total number of bars, resulting in shifts of 91–455 frames). The same image sequence was repeated 10 times with-

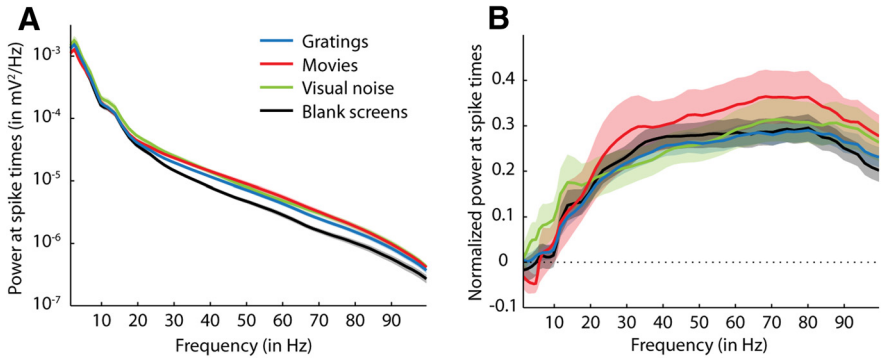

Figure 2. LFP power at the times of spikes in response to gratings (blue), movies (red), visual noise (green), and blank screens (black). ***A***, LFP power at spike times (mean ± 1 SEM across all recorded neurons; $n = 108, 43, 42$, and 78 for gratings, movies, visual noise, and blank screens, respectively). LFP power at each frequency was first averaged across all spikes of each neuron and then across all neurons. ***B***, Same data as in ***A***, but here mean LFP power at spike times is plotted in relation to mean LFP power measured during all times of stimulus presentation (complete spectrum). For each neuron, the mean LFP power of the complete spectrum is subtracted from the LFP power at each spike and divided by the SD of the complete spectrum. These normalized values were then averaged across all spikes of the same neuron and then averaged across all neurons. The dotted line at zero marks the normalized mean LFP power of the complete spectrum.

out breaks between repetitions. In total, the complete presentation of the noise stimulus lasted for ~13 min and 39 s.

Data analysis

Preprocessing of LFP. To remove very low-frequency fluctuations from the recorded LFP (low-impedance electrode), a local detrending procedure was applied (function locdetrend of MATLAB toolbox chronux, http://chronux.org, as suggested by Mitra and Bokil, 2008). It performed a linear regression on overlapping data segments of 1 s length moving in steps of 0.5 s and averaged the regression lines to obtain the fit that was then subtracted. The LFP was then filtered, first using a high-pass filter with cutoff frequency of 1 Hz and, second, using a low-pass filter with cutoff frequency of 100 Hz. Both were Butterworth filters of order 5 and were applied in the forward and reverse directions to ensure zero-phase distortion. To remove line noise, notch filters were applied to the LFP at the frequencies with maximum power ~50, 100, and 150 Hz, corresponding to the frequency of the line noise and its harmonics. The bandwidth of each notch filter was set manually for each dataset. One dataset (animal cat0310, recording site P1C1, file 3) was recorded at a sampling rate of 20 kHz and was downsampled to 1 kHz after the local detrending using the MATLAB function decimate, first with reduction factor 5 and then with reduction factor 4.

Spectral and phase analysis of LFP. Power of the LFP was measured using the multitaper method (for details, see Mitra and Bokil, 2008). Spectral estimation was averaged over two Slepian tapers. Power was estimated on small moving time windows (shifted by 50 ms) of lengths that were varied depending on frequency to allow for a good compromise between accurate power estimation and fine temporal resolution. Time widows of 1, 0.5, 0.2, and 0.15 s were used for frequencies between 1 and 5.5, 5.5 and 11, 11 and 20, and 20 and 100 Hz, respectively. To reach a constant time–bandwidth product of 1.5, the half-bandwidth of the tapers for these four frequency bands were set to 1.5, 3, 7.5, and 10 Hz, respectively. These settings are comparable to those chosen by Rasch et al. (2008). To calculate power spectra and spectrograms of the LFP the MATLAB toolbox chronux (http://chronux.org) was used.

For estimates of LFP phase in small time bins (1/4 of oscillation cycle), the LFP was filtered within bands of 2 Hz using a Kaiser window FIR filter with 60 dB attenuation in stop-bands, 0.01 dB pass-band ripple, and transition bands of 1 Hz. The Hilbert transform of the filtered LFP was then used to estimate phase in 1 ms bins. Estimates were then averaged across the appropriate number of bins. Because the FIR filters were very large (a few seconds), only data recorded at least 10 s after the start and at least 10 s before the end of each recording were considered to circumvent filter onset and offset artifacts.

To determine the mean and SD of a phase distribution and to test for its uniformity, the appropriate functions of the MatLab toolbox CircStat for statistics on circular distributions were used (Berens, 2009).

Spike sorting. Based on the recorded continuous voltage traces of the high-impedance electrode, action potentials were detected and sorted using the offline sorting algorithm WaveClus (Quiroga et al., 2004), which is a publicly available MATLAB toolbox. Before spike detection, the raw voltage traces were band-pass filtered between 200 and 3000 Hz with an elliptic filter in the forward and reverse directions to prevent phase distortions. The spikes clustered by WaveClus were checked visually for false assignments. Spikes that were not assigned to any cluster or that were discarded manually were screened for overlapping spikes originating from two neurons. Overlapping wave forms were decomposed by matching them with templates of the previously found spike clusters (Atiya, 1992). Matches were inspected manually and corrected if necessary. This procedure recovered spike occurrences that would go undetected with spike-sorting algorithms only based on the similarity between waveforms.

Strong response events. We also investigated how the LFP and its temporal relation to spikes changes when the neuron is responding to a stimulus with strongly elevated activity. We defined a spike of a neuron to fall in such a strong response event if two conditions were fulfilled. First, the average firing rate in response to the stimulus had to cross a certain threshold: the 95th percentile of the neuron's spike rate distribution measured in response to all stimuli of one class. Second, the neuron had to spike in at least 50% of all trials (or in at least 33% of all trials if the total number of trials exceeded 21) during this period of elevated firing, which eliminated events with highly unreliable responses. In the following, we will refer to spikes inside of these periods as "event spikes" as opposed to "nonevent spikes," which are all spikes outside of these periods. Our measure of strong response events is similar to the definition of response events given by Yen et al. (2007).

Results

The following analyses are based on recordings made in area 17 of 15 anesthetized adult cats. We recorded spiking activity of one to three neurons simultaneously using a high-impedance pipette and at the same time the LFP using a second pipette that had a lower impedance. Both pipettes were glued together with a tip-to-tip distance of ~30 μm. In total, we recorded the LFP together with a triplet of neurons in two cases, in 42 cases with a pair, in 27 cases together with a single neuron.

LFP power at spike times

The amplitude of LFP power at the time of a neuron's spikes reflects how strongly the activity of this neuron is related to the net activity of the surrounding neural population. An example of single trial responses to 10 presentations of a 10-s-long natural movie (Fig. 1) shows that a consistent relationship between spike times of two nearby neurons (orange and purple ticks) and LFP power (here 1–4 Hz in gray, 20–100 Hz in black) is not evident to the eye. Average power spectra measured at times of spikes (Fig. 2*A*) were very similar across all stimulus classes (drifting gratings, natural movies, and visual noise) and showed no prominent features such as clear elevations of power at a certain frequency band. When comparing LFP power averaged over the whole

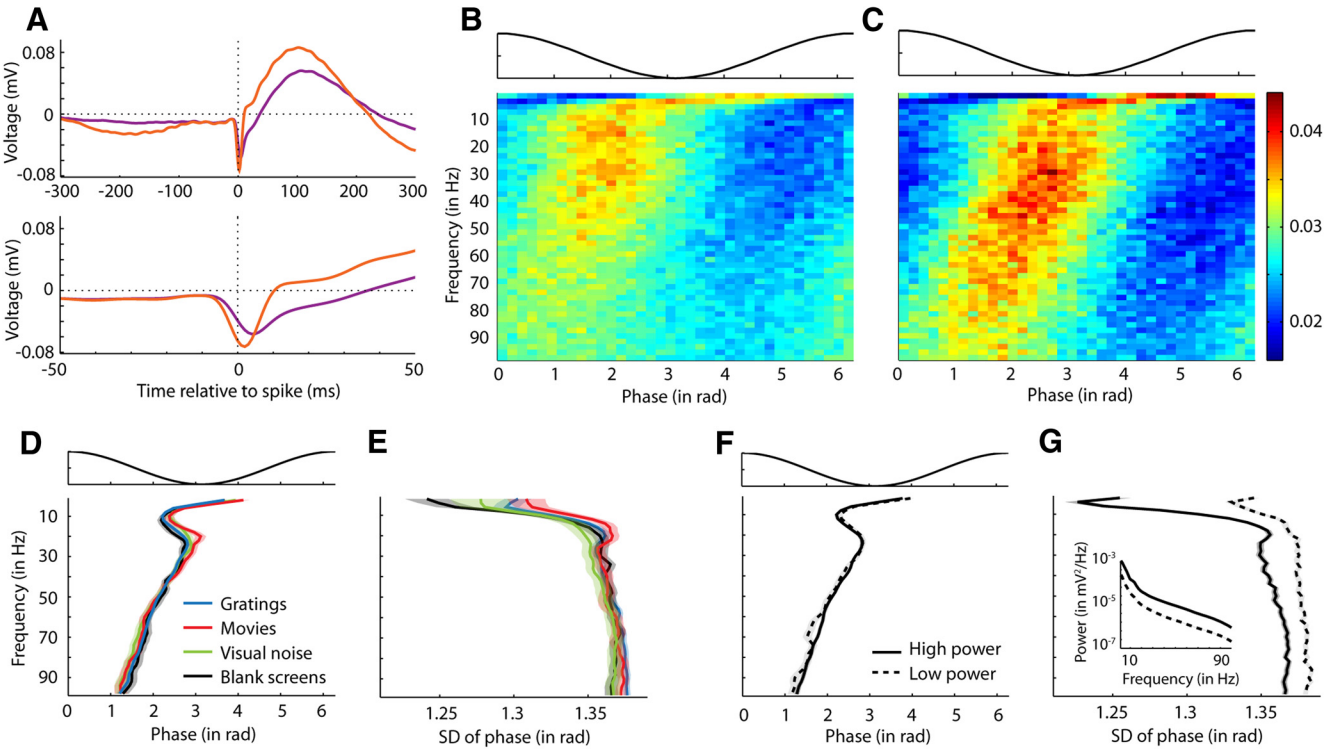

Figure 3. Relationship between LFP phase and spike times. ***A***, Example showing STAs of the LFP for two simultaneously recorded neurons (purple and orange, respectively) during the presentation of gratings (data from cat1410 P4C1). Top and bottom plots show the same data at a coarse and fine temporal scale, respectively. Dotted vertical lines at zero mark the times of spikes. One SEM plotted around the mean was smaller than the thickness of the lines ($n = 21510$ and 12511 for neuron 1 and neuron 2, respectively). ***B***, Example showing the distribution of LFP phases at spike times for neuron 1 in response to gratings based on same data as in ***A*** (purple traces). Top, Illustration of LFP phase. Bottom, For each frequency (*y*-axis), the normalized probability of a spike (*sp*) given the LFP phase (φ_k), $P(sp|\varphi_k)/\sum_i P(sp|\varphi_i)$, is illustrated by the color code (see color bar to the left of ***C***). ***C***, Same as in ***B***, but for neuron 2 based on same data as in ***A*** (orange traces). ***D***, Top, Illustration of LFP phase. Bottom, For each frequency, preferred LFP phase (mean ±1 SEM across all neurons) is plotted in response to gratings (blue), movies (red), visual noise (green), and blank screens (black). First, LFP phases at all spike times of one neuron were averaged and then across neurons. Only neurons with a distribution of LFP phases at spike times that was significantly different from uniform ($p < 0.05$, Rayleigh test for uniformity of circular data) were taken into account (total number of neurons $n = 110, 45, 41, 110$ for gratings, movies, visual noise, and blank screens, respectively). ***E***, SD of LFP phases (mean ±1 SEM across all neurons) in response to each stimulus class, respectively. All neurons were considered, including those with nonsignificant LFP phase locking. ***F***, Top, Illustration of LFP phase. Bottom, Average LFP phase (mean ±SEM across neurons and stimulus classes) for spikes occurring during time points of high LFP power (solid line) and during time points of low LFP power (dashed line). Only neurons with a nonuniform distribution of phases at spike times were considered ($n = 169–246$ and 48–193 for high and low power across frequencies, respectively). ***G***, SD of LFP phases (mean ±1 SEM across all neurons and stimulus classes) at spikes occurring during high LFP power (solid line) and low LFP power (dashed line) ($n = 265$ and 245 for high and low power, respectively). Here, all neurons were considered, not just those exhibiting significant LFP phase locking. Inset, Spectra (mean ±1 SEM across all neurons) of LFP power at spike times that occurred during time windows of high power (solid line) and of low power (dashed line). Power spectra were averaged across all spikes of each neuron and then across all neurons.

stimulation period with the power at spike times (Fig. 2*B*), no difference was detectable for frequencies up to 10 Hz. LFP power of frequencies >20 Hz, however, was on average higher at spike times (~0.25–0.3 SDs larger than the mean of the distribution of power occurring throughout stimulation). This relationship between LFP power and spiking was the same for all stimulus classes (gratings, visual noise, and natural movies). During spontaneous activity, power of high frequencies also increased during spiking, but was lower compared with power during visual stimulation (black lines in Fig. 2*A*,*B*). In summary, neurons were more likely to spike during increased power at higher frequencies (>20 Hz), whereas spiking was not correlated to changes in low-frequency power of the LFP.

Locking of spikes to LFP phases

The LFP is thought to reflect synchronized activity of neural populations and the phase of the LFP marks the oscillation period of the population oscillator (Buzsáki, 2006). Analyzing the relationship between LFP phase and spike times of single neurons reveals how precisely in time each neuron is locked to oscillations of the nearby population. Figure 3*A* shows the spike-triggered averages (STAs) of the LFP for two neighboring neurons (purple and orange traces, respectively). The spikes of both neurons occurred on average before the peak of low frequencies and approximately at or just before the trough of higher-frequency oscillations. Figure 3, *B* and *C*, give a more precise view of phase locking of spikes, in which the probability of a spike occurring at a certain LFP phase is plotted as a function of LFP frequency for each neuron. Consistent with the STAs in Figure 3*A*, spiking probability was higher before the peak of an oscillation cycle of very low frequencies, as well as before and in the trough of higher frequencies. Note also that the first neuron (Fig. 3*B*, purple trace in *A*) spiked a little earlier in the oscillation cycles of higher frequencies than the neighboring neuron, the spikes of which tended to appear closer to the trough (Fig. 3*C*, orange trace in *A*). Therefore, despite experiencing the same extracellular LFP, neighboring neurons are not thereby constrained to spike simultaneously.

We defined the preferred LFP phase of a neuron for a certain frequency as the mean LFP phase across all spike times. A neuron was said to have a preferred LFP phase for a frequency only if its spikes were significantly locked to any phase in the LFP for a given frequency. Evidence for locking would be indicated by a nonuniform distribution of LFP phases at which

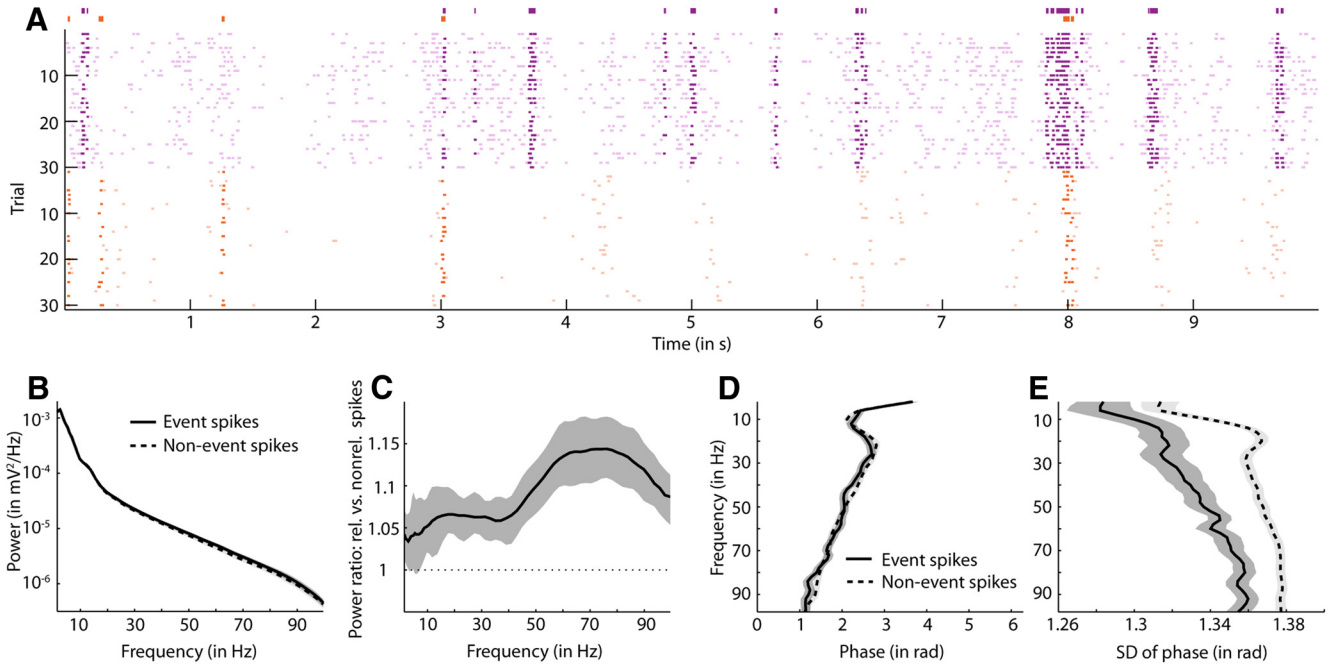

Figure 4. LFP inside and outside of strong response events. ***A***, Example showing a raster plot of spikes of two neighboring neurons (purple and orange dots, respectively) in response to 30 repetitions of a movie (cat1310 P2C2). Strong response events are marked by thick lines of the same color as the neuron's spike times above the raster plot. Spikes that occurred inside strong response events are presented in a darker color than other spikes. ***B***, LFP power (mean ±1 SEM across all neurons) at spikes inside of strong response events (solid line with dark gray shade) and spikes outside of such events (dashed line with light gray shade) ($n = 70$). For each neuron, spikes of all stimulus classes were pooled together. ***C***, Ratio between LFP power at spikes inside and outside of strong response events (mean ±1 SEM across all neurons, $n = 70$). First, the ratio between the mean power of the two groups of spikes was calculated for each neuron and then ratios were averaged across neurons. ***D***, Average LFP phase of spikes occurring inside (solid line) and outside of strong response events (dashed line) ($n = 75$). Lines and patches show the mean ±1 SEM across neurons, respectively. ***E***, SD (mean ±1 SEM across all neurons) of LFP phase at spikes inside (solid line) and outside of strong response events (dashed line).

the spikes occurred ($p < 0.05$, Rayleigh test for uniformity of circular data). The population data show that the preferred LFP phases averaged across all neurons (Fig. 3*D*) were very similar to those in our previous examples and did not differ across stimulus classes. Similarly, the average strength of phase locking (Fig. 3*E*), as measured by the circular SD, was highly similar across stimulus classes.

It is generally held that an increase in LFP power reflects greater synchrony between neurons (Buzsáki, 2006; Lindén et al., 2011), which in turn leads to greater precision in phase locking of spikes (Burns et al., 2010; Jia et al., 2013a). To investigate this relationship between LFP power and phase locking, we sorted the spikes of each neuron into two groups according to whether they occurred during high or low LFP power. LFP power was considered high if it exceeded the median power that occurred during spontaneous activity and low if it was below the median power. The inset in Figure 3*G* depicts the spectra of high and low LFP power, each averaged across all neurons. It shows that the distributions for high and low LFP powers were clearly different from one another. However, the average preferred LFP phase of all recorded neurons and for all frequencies did not change with the magnitude of LFP power (Fig. 3*F*). The average SDs of spike-triggered LFP phases for high- versus low-power epochs are shown in Figure 3*G*. Higher LFP power only marginally increased the strength of phase locking (i.e., weakly decreased the SD) for frequencies >20 Hz, but increased phase locking more strongly for frequencies <14 Hz. Nevertheless, the maximum decrease of phase SD by higher power amounted to ~1.7% of one gamma cycle.

In summary, spikes were locked to certain oscillation phases for all LFP frequencies independent of LFP power. Higher power only slightly increased the strength of phase locking.

LFP power and phase locking during strong versus weak spiking responses

Do spikes that occur during epochs of elevated responses to a stimulus have a special role? Our reason for posing this question is that strong responses of a neuron may be caused by a synchronous barrage of synaptic inputs, which naturally should be reflected in the LFP. We defined strong response events as epochs in which the mean firing rate of the neuron exceeds the 95th percentile of firing and in which the neuron emits one or more spikes in at least 1/3 of the trials so that unreliable responses are excluded. An example of spikes from two neighboring neurons emitted inside of strong response events is given in Figure 4*A*. Figure 4*B* shows that the LFP power barely differed between event spikes and nonevent spikes. On average, LFP power in the 60–80 Hz frequency band was 1.15 times higher at event spikes than at nonevent spikes (Fig. 4*C*). For frequencies up to 40 Hz, this ratio was ~1.05. The preferred LFP phases of event and nonevent spikes did not differ (Fig. 4*D*). Phase locking for event spikes was, however, somewhat stronger than for nonevent spikes, especially for frequencies between 15 and 30 Hz (Fig. 4*E*). In summary, LFP power and phase locking of event spikes tended to be stronger than for nonevent spikes. The small magnitudes of differences between event and nonevent spikes indicate, however, that the fluctuations in a single cell's synaptic input leading to event spikes are barely reflected in the LFP.

Phase locking of neighboring neurons

We then investigated whether spikes of neighboring neurons were locked to more similar LFP phases than expected from the distribution of preferred LFP phases across the whole population of neurons. Presumably, neighboring neurons are likely to get similar synaptic input but similar subthreshold membrane fluc-

tuations and therefore would be expected to lock to similar LFP phases. Figure 5 shows the differences in phase locking between neighboring neurons (solid lines) and between two neurons from two different recording sites (dashed lines) in response to each stimulus class separately. We used a permutation procedure to generate the control data (dashed lines). First, we generated as many pairs of nonneighboring neurons from different recording sessions as the number of recorded pairs of neighboring neurons. Second, the mean difference of preferred phases between the paired neurons was determined. This procedure was repeated 500 times. Dashed lines and light gray shades in each panel of Figure 5 show the mean and the 95% confidence interval of these 500 mean differences. For the large majority of frequencies, differences in preferred LFP phases between neighboring neurons fell within the confidence interval of expected differences (those between random neurons) in response to all stimulus classes. These data indicate that neurons that exhibit phase locking were not spatially clustered in primary visual cortex according to their preferred LFP phase.

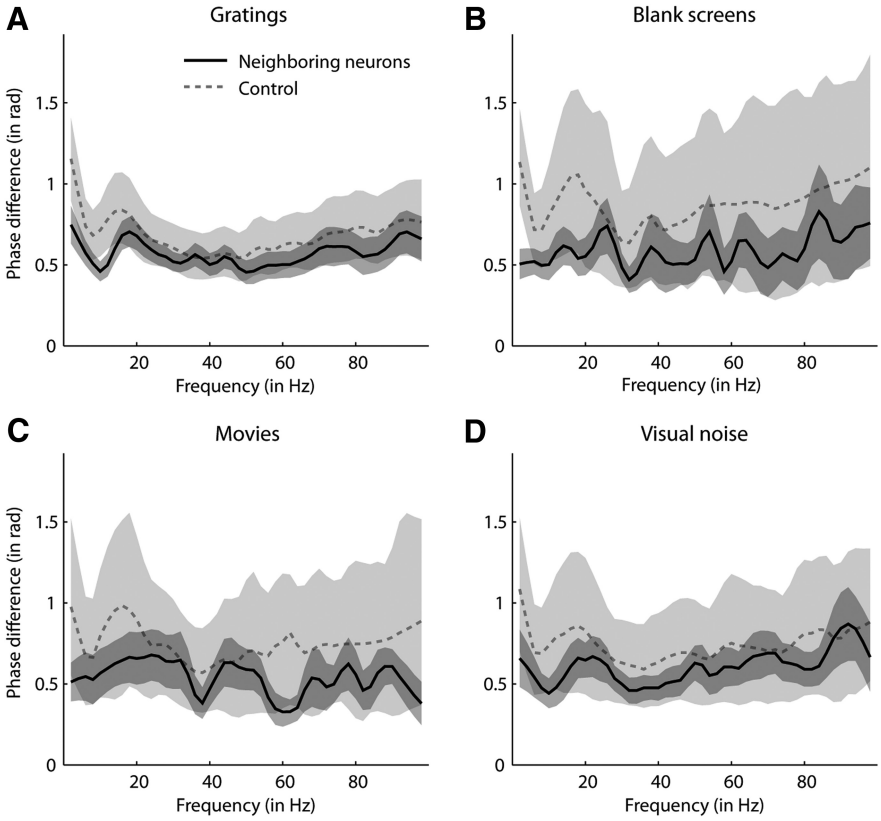

Figure 5. Differences between preferred LFP phases of neighboring neurons in response to different stimulus classes. ***A***, Solid black line with dark gray shading depicts differences between preferred phases (mean ±SEM across all pairs) of neighboring neurons in response to gratings. Only pairs for which both neurons had nonuniform distributions of phases at spike times were considered (n = 21–45 across frequencies). Dashed gray line with light gray shade shows bootstrapped mean differences between preferred phases of neurons from two different recording sites (mean and 95% confidence interval), also in response to gratings (see main text for details on bootstrap analysis). ***B–D***, Same as in ***A***, but in response to stimuli of different classes (n = 7–28, 7–14, and 8–14 for blank screens, movies, and visual noise, respectively).

Discussion

Our investigation of the temporal relationship between the LFP and spikes of nearby neurons demonstrated that spikes were more strongly phase locked at low frequencies (<14 Hz) than at high frequencies and that LFP power at high frequencies (>20 Hz) was increased at the times of spikes. This is consistent with previous observations on spike-field coherence, which reflects both amplitude covariation as well as phase consistency of spikes and the LFP (Srinath and Ray, 2014). Spike-field coherence was found to exhibit peak values at low frequencies (<10 Hz), consistent with a stronger phase locking in our data, and at gamma frequencies (~30–80 Hz), consistent with higher power at spike times in our data (Siegel and König, 2003; Henrie and Shapley, 2005; Burns et al., 2010; Ray and Maunsell, 2011b; Lashgari et al., 2012; Jia et al., 2013a). In all of these studies, peak spike-field coherence was low, never exceeding average values of 0.25 (where 1 is the maximum value), which was also reflected in our results.

On average, spikes tended to occur just before the peak of low frequencies of the LFP and just before or at the trough of higher frequencies. This agrees well with findings from multiunit activity recorded in monkey V1 (Montemurro et al., 2008; Rasch et al., 2008). In addition to these previous studies, our data showed that single neurons exhibited weak phase locking to high frequencies, but with similar preferred phases. The alternative, namely that single neurons are tightly phase locked but have widely varying preferred phases across the population, could be ruled out.

Our data also showed that, on average, the preferred phase and the strength of phase locking (i.e., the variance of spike phases) almost never changed when stimulus drive increased (i.e., when LFP power increased or when neurons spiked more strongly and reliably). Only when LFP power in the low frequencies (≤10 Hz) was high did phase locking become stronger. This was expected because neurons in the synchronized state (i.e., during high power in low frequencies) tend to increase their firing rate during the up phases of the LFP (Harris and Thiele, 2011). Conversely, the lack of change in the spike–LFP relationship in the higher frequencies does not support some hypotheses on the role of the LFP.

These hypotheses, which we will discuss below, either explicitly involve the occurrence of gamma oscillations (i.e., clear elevations of power in a narrow frequency range within 30–80 Hz) or are strongly linked to them. One goal of this study was to probe these hypotheses in the absence of prominent gamma oscillations because several studies, including ours, indicated that they do not occur in response to, for example, natural stimuli (see Introduction). Analysis of our data indeed revealed that only few stimuli (gratings) elicited gamma oscillations and then only weakly. We cannot exclude temporally restricted appearances of gamma oscillations, but they were not an obvious or reliable feature in our data.

The theory of gamma-phase decoding supposes that the spike phase encodes stimulus strength. The idea is that synchronous activity of inhibitory neurons resets the activity of excitatory cells in the local pool so that the most strongly driven excitatory cells fire first in the next gamma cycle (König et al., 1995). In this way, stimulus strength can be read out within one oscillation

cycle (Fries et al., 2007). In visual cortex of awake monkeys, spikes systematically shifted their position relative to the oscillation cycle as a function of the neuron's firing rate (Vinck et al., 2010). That study, however, only compared responses to gratings of preferred versus nonpreferred orientations, which elicit, respectively, very strong or very weak population responses. Whether the same effect occurs in response to natural stimuli, which evoke a more heterogeneous response pattern in neuronal populations (Yen et al., 2007; Martin and Schröder, 2013), remained an open question. Our results address this question directly because we investigated spike phase in response to natural stimuli and compared conditions of high versus low gamma power as well as spikes inside versus outside of strong response events. According to the gamma-phase decoding hypothesis, the spike phase should shift forward within the gamma cycle under high gamma power. This was not observed in our data. It might be argued that our results do not contradict this hypothesis directly because our stimuli did not evoke prominent gamma oscillations. However, if the hypothesis has any general relevance, then it should also apply to the natural stimuli that we used.

In addition, if spike-phase locking was used to encode stimulus information more efficiently, then it may be expected that neurons with similar stimulus preferences lock to similar phases of the LFP. In cat visual cortex, nearby neurons share more stimulus preferences than distant neurons (Hubel and Wiesel, 1962; Mante and Carandini, 2005; Rothschild and Mizrahi, 2015) and should thus share their preferred LFP phases. In contrast, our data show that the preferred phases of neighboring neurons were as different from each other as expected from the average distribution of spike phases. An interesting question for future research is whether the subset of neurons that spike during the same LFP phase form some sort of an assembly coding for similar stimulus properties or for different properties of the same object. This will require the recording of a much larger number of individual neurons together with the LFP.

The hypothesis of communication through coherence proposes that the transmission of spikes between neuronal groups is most efficient if both groups oscillate coherently and with the optimal phase delay. In this way, spikes of the sending group arrive when the receiving group is most sensitive to input. One would expect that spikes would be most strongly phase locked to the LFP when stimulus drive is strongest. The strength of phase locking should decrease with stimulus drive so that if two groups compete to communicate to a third group, the one with spikes that are more synchronized to oscillations wins because the receiving group will tend to phase lock more to those synchronized spikes (Fries, 2005). There was very little evidence for this in our data. High (broadband) gamma power decreased the SD of spike phases only marginally compared with low power, and the same held true for spikes occurring inside versus outside of strong responses events (maximum reduction of phase SD was 0.64% of one gamma cycle). It seems unlikely that such marginal differences are relevant.

A recent study reported a lack of gamma oscillations in human visual cortex in response to visual noise and natural images (Hermes et al., 2015). Brunet et al. (2014) responded by arguing that communication could occur in the absence of prominent gamma bumps as long as the coherence between the neuronal groups is strong enough. Even so, stimulus-driven neurons should strongly lock to the LFP so that their signals can be efficiently communicated to the receiver area, which was not observed in our data.

The strongest increase in phase locking from low to high LFP power was observed in the beta-frequency range (15–25 Hz). Coherence in this range is thought to play a role in interareal communication (i.e., over long-range distances; Brovelli et al., 2004; Tallon-Baudry et al., 2004; Lachaux et al., 2005). Possibly, beta oscillations could play a more important role for communication through coherence than gamma oscillations seem to.

Up to now, we have assumed that general stimulus drive is the only determinant of phase locking. An alternative view is that one stimulus causes spikes to lock to one phase whereas a different stimulus causes spikes to lock to another phase. This was observed for low-frequency oscillations of 4–8 Hz in auditory cortex of awake monkey in response to natural sounds (Kayser et al., 2009), as well as for oscillations of 1–4 Hz in primary visual cortex of anesthetized monkey in response to natural movies (Montemurro et al., 2008). A necessary prerequisite for this scenario is that not only spikes but also LFP phase must be consistently and reliably locked to the stimulus. Our data showed no such reliable locking of LFP phase to the stimulus (data not shown). It may still be conceivable that spikes are locked to different LFP phases for different stimuli, namely if they are not perfectly locked in time to the stimulus. Another possibility is that the relevant frequency for spike-phase locking is changing continuously across time. More sophisticated analyses will be necessary to explore these possibilities.

Overall, our data indicate that phase locking of spikes in the gamma frequencies has little relevance for coding or communication assuming a simple hypothesis: phase locking changes with the strength of stimulus drive in the neural population. However, we have not tested communication between neuronal ensembles or encoding by spike phase directly and can therefore not exclude that phase locking is a relevant mechanism. It could, for example, show different characteristics in awake and attending animals, that phase locking may be determined by stimulus identity, or that the relevant LFP frequency may change over time. Averaging across stimuli and across time would easily disguise such dependencies and future studies should strive to investigate the dynamics of spike-phase locking over short epochs.

References

Atiya AF (1992) Recognition of multiunit neural signals. IEEE Trans Biomed Eng 39:723–729. CrossRef Medline

Berens P (2009) CircStat: a MATLAB toolbox for circular statistics. Journal of Statistical Software 31:1–21.

Brovelli A, Ding M, Ledberg A, Chen Y, Nakamura R, Bressler SL (2004) Beta oscillations in a large-scale sensorimotor cortical network: Directional influences revealed by Granger causality. Proc Natl Acad Sci U S A 101:9849–9854. CrossRef Medline

Brunet N, Vinck M, Bosman CA, Singer W, Fries P (2014) Gamma or no gamma, that is the question. Trends Cogn Sci 18:507–509. CrossRef Medline

Brunet N, Bosman CA, Roberts M, Oostenveld R, Womelsdorf T, De Weerd P, Fries P (2015) Visual cortical gamma-band activity during free viewing of natural images. Cereb Cortex 25:918–926. CrossRef Medline

Burns SP, Xing D, Shapley RM (2010) Comparisons of the dynamics of local field potential and multiunit activity signals in macaque visual cortex. J Neurosci 30:13739–13749. CrossRef Medline

Buzsáki G (2006) Rhythms of the brain. Oxford: OUP.

Buzsáki G, Wang XJ (2012) Mechanisms of gamma oscillations. Annu Rev Neurosci 35:203–225. CrossRef Medline

Buzsáki G, Anastassiou CA, Koch C (2012) The origin of extracellular fields and currents: EEG, ECoG, LFP and spikes. Nat Rev Neurosci 13:407–420. CrossRef Medline

Frien A, Eckhorn R, Bauer R, Woelbern T, Gabriel A (2000) Fast oscillations display sharper orientation tuning than slower components of the same recordings in striate cortex of the awake monkey. Eur J Neurosci 12:1453–1465. CrossRef Medline

Fries P (2005) A mechanism for cognitive dynamics: neuronal communication through neuronal coherence. Trends Cogn Sci 9:474–480. CrossRef Medline

Fries P (2009) Neuronal gamma-band synchronization as a fundamental process in cortical computation. Annu Rev Neurosci 32:209–224. CrossRef Medline

Fries P, Reynolds JH, Rorie AE, Desimone R (2001) Modulation of oscillatory neuronal synchronization by selective visual attention. Science 291: 1560–1563. CrossRef Medline

Fries P, Nikolić D, Singer W (2007) The gamma cycle. Trends Neurosci 30:309–316. CrossRef Medline

Gieselmann MA, Thiele A (2008) Comparison of spatial integration and surround suppression characteristics in spiking activity and the local field potential in macaque V1. Eur J Neurosci 28:447–459. CrossRef Medline

Gray CM, Singer W (1989) Stimulus-specific neuronal oscillations in orientation columns of cat visual cortex. Proc Natl Acad Sci U S A 86:1698–1702. CrossRef Medline

Gray CM, König P, Engel AK, Singer W (1989) Oscillatory responses in cat visual cortex exhibit inter-columnar synchronization which reflects global stimulus properties. Nature 338:334–337. CrossRef Medline

Harris KD, Thiele A (2011) Cortical state and attention. Nat Rev Neurosci 12:509–523. CrossRef Medline

Haslinger R, Pipa G, Lima B, Singer W, Brown EN, Neuenschwander S (2012) Context matters: the illusive simplicity of macaque V1 receptive fields. PLoS One 7:e39699. CrossRef Medline

Henrie JA, Shapley R (2005) LFP power spectra in V1 cortex: the graded effect of stimulus contrast. J Neurophysiol 94:479–490. CrossRef Medline

Hermes D, Miller KJ, Wandell BA, Winawer J (2015) Stimulus dependence of gamma oscillations in human visual cortex. Cereb Cortex 25:2951–2959. Medline

Hubel DH, Wiesel TN (1962) Receptive fields, binocular interaction and functional architecture in the cat's visual cortex. J Physiol 160:106–154. CrossRef Medline

Jia X, Kohn A (2011) Gamma rhythms in the brain. PLoS Biol 9:e1001045. CrossRef Medline

Jia X, Tanabe S, Kohn A (2013a) Gamma and the coordination of spiking activity in early visual cortex. Neuron 77:762–774. CrossRef Medline

Jia X, Xing D, Kohn A (2013b) No consistent relationship between gamma power and peak frequency in macaque primary visual cortex. J Neurosci 33:17–25. CrossRef Medline

Kayser C, Salazar RF, Konig P (2003) Responses to natural scenes in cat V1. J Neurophysiol 90:1910–1920. CrossRef Medline

Kayser C, Montemurro MA, Logothetis NK, Panzeri S (2009) Spike-phase coding boosts and stabilizes information carried by spatial and temporal spike patterns. Neuron 61:597–608. CrossRef Medline

König P, Engel AK, Roelfsema PR, Singer W (1995) How precise is neuronal synchronization? Neural Comput 7:469–485. CrossRef Medline

Lachaux JP, George N, Tallon-Baudry C, Martinerie J, Hugueville L, Minotti L, Kahane P, Renault B (2005) The many faces of the gamma band response to complex visual stimuli. Neuroimage 25:491–501. CrossRef Medline

Lashgari R, Li X, Chen Y, Kremkow J, Bereshpolova Y, Swadlow HA, Alonso JM (2012) Response properties of local field potentials and neighboring single neurons in awake primary visual cortex. J Neurosci 32:11396–11413. CrossRef Medline

Lindén H, Tetzlaff T, Potjans TC, Pettersen KH, Grün S, Diesmann M, Einevoll GT (2011) Modeling the spatial reach of the LFP. Neuron 72: 859–872. CrossRef Medline

Mante V, Carandini M (2005) Mapping of stimulus energy in primary visual cortex. J Neurophysiol 94:788–798. CrossRef Medline

Martin KA, Schröder S (2013) Functional heterogeneity in neighboring neurons of cat primary visual cortex in response to both artificial and natural stimuli. J Neurosci 33:7325–7344. CrossRef Medline

Mitra PP, Bokil H (2008) Observed brain dynamics. Oxford: OUP.

Montemurro MA, Rasch MJ, Murayama Y, Logothetis NK, Panzeri S (2008) Phase-of-firing coding of natural visual stimuli in primary visual cortex. Curr Biol 18:375–380. Medline

Nelson MJ, Pouget P (2010) Do electrode properties create a problem in interpreting local field potential recordings? J Neurophysiol 103: 2315–2317. CrossRef Medline

Quiroga RQ, Nadasdy Z, Ben-Shaul Y (2004) Unsupervised spike detection and sorting with wavelets and superparamagnetic clustering. Neural Comput 16:1661–1687. CrossRef Medline

Rasch MJ, Gretton A, Murayama Y, Maass W, Logothetis NK (2008) Inferring spike trains from local field potentials. J Neurophysiol 99:1461–1476. CrossRef Medline

Ray S, Maunsell JH (2011a) Different origins of gamma rhythm and high-gamma activity in macaque visual cortex. PLoS Biol 9:e1000610. CrossRef Medline

Ray S, Maunsell JH (2011b) Network rhythms influence the relationship between spike-triggered local field potential and functional connectivity. J Neurosci 31:12674–12682. CrossRef Medline

Rothschild G, Mizrahi A (2015) Global order and local disorder in brain maps. Annu Rev Neurosci 38:247–268. CrossRef Medline

Siegel M, König P (2003) A functional gamma-band defined by stimulus-dependent synchronization in area 18 of awake behaving cats. J Neurosci 23:4251–4260. Medline

Srinath R, Ray S (2014) Effect of amplitude correlations on coherence in the local field potential. J Neurophysiol 112:741–751. CrossRef Medline

Tallon-Baudry C, Mandon S, Freiwald WA, Kreiter AK (2004) Oscillatory synchrony in the monkey temporal lobe correlates with performance in a visual short-term memory task. Cereb Cortex 14:713–720. CrossRef Medline

van Hateren JH, Ruderman DL (1998) Independent component analysis of natural image sequences yields spatio-temporal filters similar to simple cells in primary visual cortex. Proc Biol Sci 265:2315–2320. CrossRef Medline

Victor JD (1992) Nonlinear systems analysis in vision: overview of kernel methods. Boca Raton, FL: CRC.

Vinck M, Lima B, Womelsdorf T, Oostenveld R, Singer W, Neuenschwander S, Fries P (2010) Gamma-phase shifting in awake monkey visual cortex. J Neurosci 30:1250–1257. CrossRef Medline

Womelsdorf T, Schoffelen JM, Oostenveld R, Singer W, Desimone R, Engel AK, Fries P (2007) Modulation of neuronal interactions through neuronal synchronization. Science 316:1609–1612. CrossRef Medline

Yen SC, Baker J, Gray CM (2007) Heterogeneity in the responses of adjacent neurons to natural stimuli in cat striate cortex. J Neurophysiol 97: 1326–1341. Medline